



Low-temperature gas-phase oxidation of diethyl ether: Fuel reactivity and fuel-specific products

Luc-Sy Tran, Olivier Herbinet, Yuyang Li, Julia Wullenkord, Meirong Zeng,
Eike Bräuer, Fei Qi, Katharina Kohse-Höinghaus, Frédérique Battin-Leclerc

► To cite this version:

Luc-Sy Tran, Olivier Herbinet, Yuyang Li, Julia Wullenkord, Meirong Zeng, et al.. Low-temperature gas-phase oxidation of diethyl ether: Fuel reactivity and fuel-specific products. Proceedings of the Combustion Institute, 2018, 37, pp.511-519. 10.1016/j.proci.2018.05.135 . hal-01922883

HAL Id: hal-01922883

<https://hal.science/hal-01922883>

Submitted on 14 Nov 2018

HAL is a multi-disciplinary open access archive for the deposit and dissemination of scientific research documents, whether they are published or not. The documents may come from teaching and research institutions in France or abroad, or from public or private research centers.

L'archive ouverte pluridisciplinaire **HAL**, est destinée au dépôt et à la diffusion de documents scientifiques de niveau recherche, publiés ou non, émanant des établissements d'enseignement et de recherche français ou étrangers, des laboratoires publics ou privés.

Low-temperature gas-phase oxidation of diethyl ether: Fuel reactivity and fuel-specific products

Luc-Sy Tran^{a,b,c}, Olivier Herbinet^b, Yuyang Li^d, Julia Wullenkord^a, Meirong Zeng^d,
Eike Bräuer^a, Fei Qi^d, Katharina Kohse-Höinghaus^a, Frédérique Battin-Leclerc^b

^a *Department of Chemistry, Bielefeld University, Universitätsstraße 25, D-33615 Bielefeld, Germany*

^b *Laboratoire Réactions et Génie des Procédés (LRGP), CNRS, Université de Lorraine, ENSIC, 1, rue Grandville, BP 20451, 54001 Nancy Cedex, France*

^c *Université de Lille, CNRS, UMR 8522 - PC2A - Physicochimie des Processus de Combustion et de l'Atmosphère, F-59000 Lille, France*

^d *School of Mechanical Engineering, Shanghai Jiao Tong University (SJTU), Shanghai 200240, PR China*

Published in Proceedings of the Combustion Institute
<https://doi.org/10.1016/j.proci.2018.05.135>

Abstract

Diethyl ether (DEE) has been recently suggested as a potential biofuel for compression-ignition engines that are known to be significantly controlled by low-temperature (LT) chemistry. However, the LT oxidation of DEE has not fully been understood in term of the formation of LT fuel-specific products. We have thus studied the oxidation of DEE by examining detailed profiles of its oxidation products under LT conditions (400–1100 K). To this end, we have used a dedicated experimental setup including a nearly-atmospheric jet-stirred reactor (JSR) coupled to online gas chromatography (GC). The experiments were complemented by measurements made with a JSR coupled to tunable synchrotron vacuum ultraviolet (SVUV) photoionization (PI) molecular-beam mass spectrometry (MBMS) for a cross-validation of the identification of important LT species.

Experimental results indicate that DEE is very reactive; it starts to react around 425 K. DEE exhibits an unusual oxidation behavior with two negative temperature coefficient (NTC) zones in the JSR study. Because of this two-NTC observation, additional experiments were performed with a plug flow reactor (PFR) combined with electron ionization (EI)-MBMS, confirming this behavior in the two types of reactor. Moreover, about 20 oxidation species in C₁-C₄ range were detected with several intermediates containing 2-3 O-atoms. Acetic acid is found to peak at 525 K with a very large amount, suggesting that it is a key species in the early stage of DEE's LT oxidation. Possible DEE-consumption paths leading to acetic acid formation could play an important role in the oxidation mechanism of DEE. A new model is proposed based on the present experimental observations to include new primary LT reaction paths. The model reproduces the experimental phenomena quite well and enhances the understanding of the two-NTC-zone occurrence and of intermediates containing 2-3 O-atoms during the LT oxidation of DEE.

Keywords: Biofuel; Diethyl ether; Low-temperature oxidation; Dual NTC zone phenomenon; Detailed kinetic model

1. Introduction

Diethyl ether (DEE, $C_4H_{10}O$) has been proposed as a promising biofuel for compression-ignition engines [1] and as an excellent ignition improver for homogeneous charge compression ignition engines [2]. These engines are known to be significantly controlled by low-temperature (LT) chemistry. A deeper understanding of DEE's LT oxidation chemistry is therefore desirable. Several experimental studies were recently performed regarding the high-temperature (HT) oxidation of DEE, e.g., ignition delay times (IDTs) [3,4], flame speeds [5,6], and species profiles [3,5,7,8]. However, experimental studies with detailed species profiles for its LT gas-phase oxidation chemistry are surprisingly scarce. Early work of Salooja [9] has reported limited species data at different pre-ignition stages in a quartz chamber for a fuel-rich DEE-air mixture. Oscillatory cool flames in DEE/ O_2 / N_2 mixtures were studied in [10], without providing species profiles. Slow oxidation (< 425 K) of DEE addressing storage-safety problems has also been studied [11-13]. Recently, IDTs of DEE were measured [4] in a rapid compression machine at 253-1317 kPa for various equivalence ratios. Moreover, the LT oxidation of DEE was increasingly investigated by model predictions [14-17]. Sakai et al. [14] developed a model including LT reactions using rate coefficients calculated in their previous work [18] for unimolecular reactions derived from the first O_2 addition, whereas rate coefficients for reactions from second O_2 addition were estimated by analogy to those of the first O_2 addition or to those of species with similar structures. Hu et al. [15] used this LT reaction subset in their model without modification. Tang et al. [16] improved a model of Yasunaga et al. [3] by mostly including important LT reactions proposed in [14,18]. Independently, Eble et al. [17] proposed a model using kinetic data empirically estimated or based on dimethyl ether reactions.

Experimental LT data of DEE, however, especially detailed species profiles, remain very scarce. Here, we have thus measured detailed profiles of oxidation products of DEE in a temperature range of 400–1100 K, providing useful data to analyze and understand details of the reaction mechanism in this technically relevant temperature regime.

2. Experiments

In the present experiments, we used two types of reactors, i.e., a jet-stirred reactor (JSR) and a plug flow reactor (PFR), and three analytical techniques: online gas chromatography (GC), tunable synchrotron vacuum ultraviolet photoionization molecular-beam mass spectrometry (SVUV-PI-MBMS), and electron ionization (EI)-MBMS.

2.1. JSR-GC experiment

Species mole fraction profiles were measured in an atmospheric JSR directly connected to GCs at the LRGP-Nancy that was previously described in [19]. The reactor (81.2 cm³ volume) is made of fused silica and heated electrically. The GCs were fitted with different columns (Carbosphere, PlotQ, and HP-5 columns) and detectors, i.e., a thermal conductivity detector (TCD), a flame ionization detector (FID)/methanizer for quantification, and a mass spectrometric detector (MS) with electron ionization at 70 eV for identification. The GC-loop/injector temperature was reduced from the usual value of 523 K to 423 K to avoid DEE pre-reactions. Calibrations were performed using cold-gas mixtures when available. For other species, calibration factors were

assumed relying on hydrogenation by the methanizer, to be identical to those of the alkanes with the same number of carbon atoms, with an uncertainty < 15%.

Flow rates of liquid DEE (Sigma-Aldrich, purity $\geq 99.7\%$) were controlled using a Coriolis flow controller followed by an evaporator set to 400 K. Experiments were performed for a mixture DEE/O₂/He with equivalence ratio $\phi = 1$, initial mole fraction 0.01/0.06/0.93, residence time of 2 s, temperature range of 400–1100 K, and pressure of 106.7 kPa.

2.2. JSR- SVUV-PI-MBMS experiment

To cross-validate the GC identification of species containing 2-3 oxygens (key LT intermediates), photoionization efficiency (PIE) spectra were measured with SVUV-PI-MBMS coupled to a JSR, located at the Hefei National Synchrotron Radiation Laboratory. Similar operating conditions were used, but replacing He by Ar that served as a reference in the SVUV-PI-MBMS data evaluation. The apparatus has been described elsewhere [20]. Gas samples were extracted from the JSR by a quartz sampling cone. The resulting molecular beam was then intersected and ionized by the tunable synchrotron VUV light. The ions were transferred by an ion guide to a home-made reflectron time-of-flight mass spectrometer (TOF-MS) with a mass-resolving power ($m/\Delta m$) ~ 2500 . The PIE spectra were measured in a photon energy range of 8–11.5 eV, with uncertainties in the determination of ionization energies of ± 0.05 and ± 0.10 eV for strong and poor signal-to-noise ratio, respectively.

2.3. PFR-EI-MBMS experiment

Because of the unusual oxidation behavior with two negative-temperature-coefficient (NTC) zones observed in the JSR experiments, additional experiments were performed in a PFR coupled with EI-MBMS at Bielefeld University. The setup has been described in [21]. The reactor consists of a fused silica tube (8 mm inner diameter, 1.40 m length) and was electrically heated. Oxidation products were sampled at the reactor exit with a quartz nozzle (~ 50 μm orifice diameter). The sampled gases were directed through a copper skimmer to the ion source of the mass spectrometer. Chemical species were ionized with an electron beam of 17 eV and accelerated into the reflectron TOF-MS with a mass resolution of $m/\Delta m \sim 2200$. Evaluation procedures were previously reported in [21] and are associated with uncertainties for major species of $\sim 15\%$ and factors of 2–4 for intermediate species.

A mixture DEE/O₂/Ar (0.005/0.030/0.965) was used with $\phi = 1$, total flow of 0.5 slm, initial gas velocity of 0.23 m/s at 373 K, and pressure of 97 kPa (temperature-dependent residence time of ~ 2 –4 s). Liquid DEE (VWR Chemicals, purity $\geq 99.7\%$) was delivered with a dialysis pump and evaporated at 373 K. Carbon balances for both JSR and PFR experiments were checked to be close to 100%.

3. Model development and simulation method

Recent DEE models [14–17] cannot satisfactorily reproduce the present experimental data. To contribute to the interpretation of this data, we have therefore attempted to develop a new LT oxidation sub-mechanism of DEE. It includes usual LT reaction classes (as considered in the above literature models) and new reaction classes that were suggested from the present experimentally-

detected species. This LT sub-mechanism was coupled to the model developed previously only for HT DEE chemistry [5], and implemented into the most recent core model of the NUI-Galway group [19]. The complete model consists of 3540 reactions involving 748 species; it is available in CHEMKIN format in Supplemental Material 1 (SM1).

The newly-proposed LT sub-mechanism of DEE includes 31 main reaction classes with details available in SM2. Only main features are presented here. The addition of O₂ to the fuel radicals (first O₂ addition) is the first step in the LT chain-branching process to form ethoxyethylperoxy radicals (ROO); the rate coefficients of this reaction class were determined using the original kinetic data (including thermochemistry) proposed by Sakai et al. [14], expecting thus a good consistency with the original source. The order of magnitude of these rate coefficients is in the range of those proposed for DME and n-pentane chemistry (compare the core mechanism). The kinetic data of bimolecular reactions following this first step were estimated based on reactions proposed for LT oxidation of di-n-butyl ether (DBE) [22]. Note that the effect of ether function in DBE is quite similar to that in DEE, e.g., close bond dissociation energies of C_α-H (~95 kcal mol⁻¹) and C_α-O (~87 kcal mol⁻¹) bonds (C_α is the carbon bonded to O atom) [5,22]. Kinetic data of ROO isomerization to hydroperoxyl-fuel radicals (QOOH) and of unimolecular reactions of these latter radicals were taken from calculations of Sakai et al. [18]. However, to improve the prediction of DEE reactivity at 500–550 K, we used averaged rate coefficients between those calculated by Sakai et al. [18] and those proposed empirically by Eble et al. [17] for the reaction $\text{CH}_3\text{CHOCH}(\text{OOH})\text{CH}_3 \rightarrow \text{CH}_3\text{CHO} + \text{CH}_3\text{CHO} + \text{OH}$.

Rate coefficients of the second O₂ addition forming the OOQOOH radicals were estimated based on the first O₂ addition. Kinetic data of OOQOOH isomerization followed by a fast O-O β-scission to form ketohydroperoxides, and decomposition of the latter species were determined following Thion et al. [22]. Indications from the present experiments (see Section 4) led us to consider new reaction classes for LT DEE oxidation illustrated in Figure 1. The rate-determining step in the Korcek decomposition process proposed by Jalan et al. [23] was used for path i in Figure 1. As a first approximation, kinetic data of path ii was taken from theoretical calculations by Wang et al. [24] for a structurally-similar species (OCH₂OCH=O) with an activation energy reduced by 2 kcal mol⁻¹ to consider the difference in bond dissociation energies between tertiary- and secondary-carbon positions, and without any modification of the proposed pre-exponential factor. This data was estimated at the high-pressure limit to keep it consistent with those of competitive paths. More accurate determination of these rate coefficients remains an interesting subject needing theoretical investigations that are beyond the scope of the present study. Note that the path ii supplies the reactive radical CH₃CO, increasing also the system reactivity. Rate coefficients of reactions in path iii were estimated mainly based on rate rules [25]. These reaction classes were not included in the DEE literature models [14–17].

Most thermochemical data of fuel, fuel radicals, and newly-involved species in LT reactions were obtained from previous quantum chemistry calculations [5,14]. Otherwise, such data were calculated using the group additivity method implemented in the RMG program [25].

Simulations of JSR data were performed using the “Perfectly_Stirred_Reactor” module of OpenSMOKE++ [26] with isothermal-constant pressure approach, whereas a multi-zone non-isothermal solution was applied following [21] for PFR simulations. The present model, after including LT reactions, was successfully examined against HT data [3–5,7] (details given in SM2).

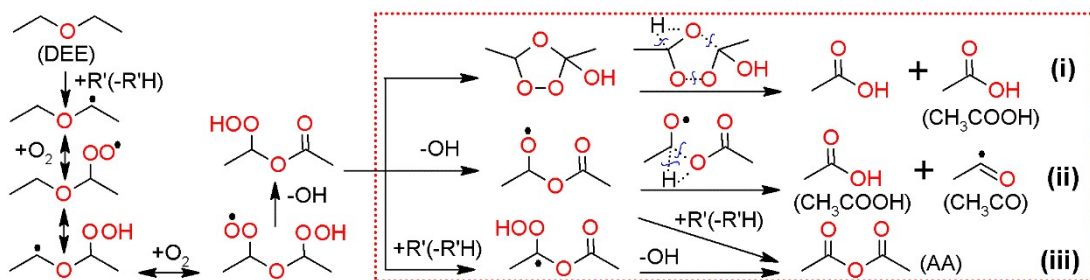


Figure 1: Examples of the newly-considered reaction classes (in dashed box) for the DEE LT sub-mechanism, leading to the formation of experimentally-detected species, e.g., acetic acid (CH_3COOH) and acetic anhydride (AA).

4. Results and discussion

4.1. Fuel reactivity and observation of two NTC zones

Figure 2a,b presents the mole fraction profiles of DEE obtained in JSR-GC (a) and PFR-EI-MBMS (b) experiments as function of temperature, together with predictions by three models (present, Eble [17], and Sakai [14] models). For clarity, other models (Hu et al. [15], Tang et al. [16]) were not included, but their prediction performance is comparable to that of the Sakai model [14] because kinetic data of LT reactions in these models are from the same source.

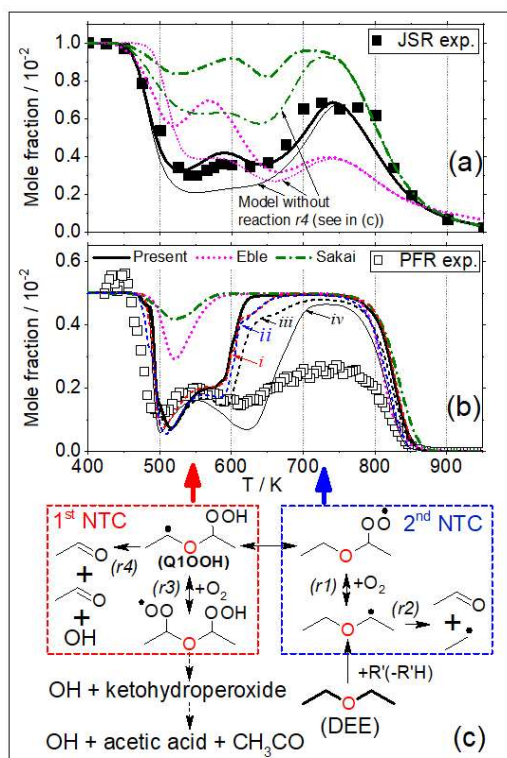


Figure 2: DEE conversion as a function of reaction temperature in two reactor types: JSR (a) and PFR (b), and proposed mechanism resulting in two NTC zones (c). In (a) and (b): symbols: experiments; lines: present (solid), Eble [17] (dotted), Sakai [14] (dash-dotted) models. In (a): thin lines: model without reaction r_4 in (c). In (b): PFR simulations using the present model with including individual uncertainties of temperature (i), pressure (ii), rate coefficients of $\text{DEE} + \text{C}_x\text{H}_y\text{O}_2$ (iii), and simultaneous inclusion of these uncertainties (iv).

Figure 2a,b shows that DEE starts to react at quite low temperature (~ 425 K). Importantly, it exhibits an unusual oxidation behavior with two NTC zones observed in both experiments. The two-NTC behavior is also evident in the profile shape of some products (including CO and CH_2O) that show two peaks in the two highest LT fuel conversion zones (further details given in SM2). The DEE conversion profile is composed of five zones. DEE is quickly consumed up to 70% at very low temperature, 425–550 K in the JSR (PFR: 425–500 K). The first NTC occurs until 600 K (PFR: 550 K), whereafter DEE's reactivity increases again until ~ 650 K. The second NTC and a decrease in fuel reactivity is seen until ~ 750 K. Finally, the reactivity rises again, and DEE is totally consumed above 950–1000 K. All three presented models show a two-NTC-zone behavior under JSR conditions, but only the present model can quantitatively predict the DEE conversion for the studied conditions. Model analyses with these models indicate the same origin of the two-NTC behavior, which is extensively explained in the coming paragraph. Under PFR conditions, all three models significantly under-predict DEE conversion, especially between ~ 600 –800 K, while the experiment shows the unambiguous presence of intermediate species (see SM2). The present model still predicts two-NTC behavior and well reproduces the first NTC, however. To further inspect the PFR discrepancies, we performed simulations assuming an uncertainty of $\sim 5\%$ in temperature (by reducing the heat transfer coefficient by a factor of 2), 5% in pressure, or a factor of 2 for rate coefficients of H-abstractions from DEE by $\text{C}_x\text{H}_y\text{O}_2$ radicals. The latter reaction class was chosen for the PFR test because it is important for the DEE conversion in the range of 600–800 K, and its estimated rate coefficients have potentially high uncertainties, and modifications of these rate coefficients affect only moderately the JSR simulations. Results (profiles i, ii, iii in Figure 2b, respectively) show that the individual effect of the tested uncertainties on DEE consumption is limited (~ 5 –12% at ~ 625 K). Including all three uncertainty sources (profile iv) significantly enhances DEE conversion, especially in the second NTC zones (up to 90% at ~ 625 K), improving the model-experiment agreement, showing the delicate temperature-sensitive reaction behavior. Remaining discrepancies at higher temperatures indicate influences of other error sources. Note that the tested uncertainties do not significantly affect the first NTC zone.

Figure 2c aims to explain the occurrence of the two NTC zones based on the fuel's structure. Only reaction paths via H-abstractions at C_α of DEE are shown because they are main consumption routes of DEE (see Section 4.2), and mostly control the fuel reactivity. The second NTC of DEE results from the competition between the first O_2 addition to the fuel radicals (reaction r1 in Figure 2c) and the decomposition of these radicals (reaction r2). The first NTC is unusual, mainly resulting from a competition between the second O_2 addition (reaction r3) and the C–O/O–O β -scission succession of the hydroperoxyl-fuel radical (Q10OH) (reaction r4). Reaction r3 is favored at LT, and its subsequent reactions are chain-branching steps because they lead to formation of reactive species, such as an OH radical and ketohydroperoxide, which decomposes easily to form a second OH radical and other small radicals such as CH_3 and CH_3CO . In contrast, reaction r4 inhibits the system's reactivity because this reaction produces only one OH radical and two stable acetaldehyde molecules. The first NTC is significantly suppressed when reaction r4 is excluded in the simulation with the three presented models (thin lines in Figure 2a). For further demonstration, sensitivity analyses for JSR DEE consumption at 560 K (in the first NTC zone) and at 700 K (in the second NTC zone) were performed using these three models, showing the important role of reactions r4 and r2 in the first and second NTC zones, respectively (more details available in SM2). With increasing temperature (~ 575 –625 K), the formed CH_3CO radicals can react and supply reactive species increasing again the system's reactivity. Indeed, near 600 K, CH_3CHO is significantly consumed and produces CH_3CO that reacts then with O_2 leading to CH_3CO_3 .

The latter radical reacts with DEE (increasing the system reactivity) and other species (e.g., HO_2 , CH_3CHO) producing $\text{CH}_3\text{CO}_3\text{H}$ (peroxyacetic acid) that decomposes to form OH (increasing the system reactivity). Moreover, temperature-dependent OH production rates show that their sum is consistent with the DEE reactivity described above. OH production increases with temperature between 450 and 550 K mainly by formation/decomposition paths of DEE-specific ketohydroperoxides, between 600 and 650 K by decomposition of $\text{CH}_3\text{CO}_3\text{H}$, $\text{CH}_3\text{O}_2\text{H}$ and $\text{C}_2\text{H}_5\text{O}_2\text{H}$, and after a transition to HT chemistry above 750 K by H_2O_2 decomposition (further details in SM2).

Note that no first NTC zone has been observed in the LT oxidation of the corresponding five-heavy-atom hydrocarbon (*n*-pentane) because the succession of β -scissions (similar to r4) in the case of *n*-pentane oxidation is energetically less favored due to the absence of the ether function, and therefore cannot compete with the second O_2 addition (similar to r3) in the LT range. Furthermore, the first NTC zone was also not observed for dimethyl ether (DME). DME only has primary carbon atoms, inducing stronger C–H bonds. It is significantly less reactive and starts to react at much higher temperatures. For further demonstration, simulations were performed for DME and *n*-pentane (using the present core model originated from [19]) at the same conditions, showing that both DME and *n*-pentane only react at higher temperatures (≥ 550 K) (see SM2). The occurrence of a two-NTC-zone behavior is therefore only likely for a fuel such as DEE that presents simultaneously an ether function and high reactivity at LT.

Note that Thion et al. [22] have also observed two-NTC-zone behavior for DBE, a molecule satisfying both abovementioned criteria. They explained the first NTC zone by a difference in temperature dependence of formation/consumption reactions of a DBE-specific ketohydroperoxide, $\text{C}_3\text{H}_7\text{C}(=\text{O})\text{OCH}(\text{OOH})\text{C}_3\text{H}_7$, produced through the second O_2 addition process, and propylhydroperoxide, $\text{C}_3\text{H}_7\text{OOH}$, produced via some subsequent steps in the ketohydroperoxide's decomposition. Their explanation differs from our analysis for DEE. Because of differences in the used conditions and in the species distribution between DEE and DBE, the origin of the unusual chemistry with two-NTC behavior could be different for these two ethers. This highly interesting oxidation behavior thus needs further comprehensive studies.

4.2. Fuel-specific intermediate species

For an overview, peak mole fractions of selected intermediates measured in the oxidation of DEE are summarized in Table S2 (SM2); they are reported together with the temperatures at which they occur, typically in the range ~ 480 – 900 K. Several categories of species are observed based on experimental data. First, species reaching maximum mole fraction above 800 K are mostly hydrocarbons including methane (CH_4), ethylene (C_2H_4), ethane (C_2H_6), and propene (C_3H_6), produced via either HT chemistry or secondary reactions. Second, species with peaks in the intermediate temperature range of 550–750 K include formaldehyde (CH_2O), acetaldehyde (CH_3CHO), ethanol ($\text{C}_2\text{H}_5\text{OH}$), ethyl vinyl ether ($\text{C}_4\text{H}_8\text{O}$, EVE), and 2-methyl-1,3-dioxolane ($\text{C}_4\text{H}_8\text{O}_2$ -cy). Finally, several species exhibit peak mole fraction below 550 K including intermediates with 2-3 O-atoms such as acetic acid (CH_3COOH), methyl formate (CH_3OCHO), ethyl formate ($\text{C}_3\text{H}_6\text{O}_2$, EF), and acetic anhydride ($\text{C}_4\text{H}_6\text{O}_3$, AA). Note that some of these species exhibit corrosive or toxic potential such as acetic acid and acetic anhydride. Besides complete JSR and PFR datasets provided in SM3, full profiles of selected species are presented here. Simulations of the experimental species profiles are overall acceptable in both reactors, even in the PFR at

temperatures outside the second NTC zone in which deviations are related to the previously discussed significant under-prediction of the fuel consumption.

Figure 3a–c presents intermediates containing 0-1 O-atom. While profiles of CH_4 , C_2H_6 (a), EVE, C_3H_6 (c) show mostly a unimodal behavior, those of several species, including $\text{C}_2\text{H}_5\text{OH}$ (a), CH_2O , C_2H_4 , and CH_3CHO (b) have bimodal or multimodal behavior, indicating their more complex formation. The present model captures most of these trends well although some discrepancies between model and experiment are noted for a few species, such as EVE. A model analysis shows that EVE is formed via HO_2 elimination of ethoxyethylperoxy radicals or by H-abstractions from fuel radicals by O_2 or HO_2 . The estimated rate coefficients for the latter reaction class could contain high uncertainties, potentially resulting in EVE under-prediction. $\text{C}_2\text{H}_5\text{OH}$ (a well-known product of HT DEE decomposition) was also detected at low temperature (Figure 3a), indicating LT-chemistry contributions to $\text{C}_2\text{H}_5\text{OH}$ formation. Toxic aldehydes (CH_2O and CH_3CHO) are formed not unexpectedly in high amounts over a large range of temperatures. This latter undesirable trend was also previously observed under flame conditions [5].

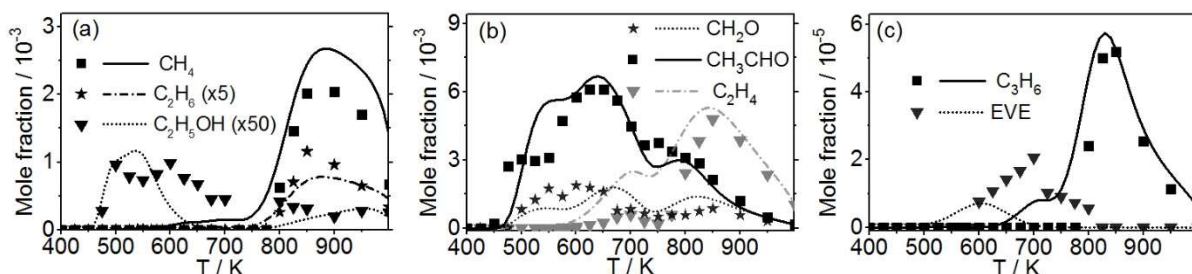


Figure 3: Mole fraction profiles of selected intermediates containing 0-1 O-atom. Symbols: JSR-GC experiment; lines: present model. An analogous figure for those from the PFR-EI-MBMS experiment is available in SM2.

More importantly, intermediates containing 2-3 O-atoms merit a closer inspection because they have been identified in the present study as key specific species of DEE's LT chemistry. Figure 4a–f presents mole fraction profiles of these species. While at higher temperatures acetaldehyde shows as a major intermediate (as mentioned earlier), acetic acid (CH_3COOH , Figures 4a and d) peaks at much lower temperature (~ 500 – 525 K, at the highest LT conversion of DEE) and was measured with high mole fractions (of ~ 10 – 3) in both JSR and PFR, which is by a factor of ~ 10 – 100 more abundant than other species containing 2-3 O-atoms formed in this low temperature range. This fact suggests that this acid could be a key species at early stage of the DEE LT oxidation, and the possible DEE consumption paths leading to acetic acid formation could play important roles in its oxidation mechanism. This explains our consideration of new reaction classes leading to the formation of CH_3COOH in the present model (see Section 3). For cross-validation in identifying intermediates containing 2-3 O-atoms, we used SVUV-PI-MBMS besides GC-MS, expecting thus a high confidence in the detection of these important species. Figure 5 shows exemplarily PIE curves measured at 500 K for species with $m/z = 60$, 88, and 102. These PIE spectra show clear onsets near the ionization energy (IE) of acetic acid (~ 10.65 eV [27]) (Figure 5a), 2-methyl-1,3-dioxolane (~ 9.46 eV), and ethyl acetate (~ 10.01 eV [27]) (Figure 5b), as well as acetic anhydride (~ 10.0 eV [27]) (Figure 5c), clearly indicating production of these species in DEE oxidation. Note that in the absence of literature data, the IE of 2-methyl-1,3-dioxolane was theoretically calculated using the procedure described in [28].

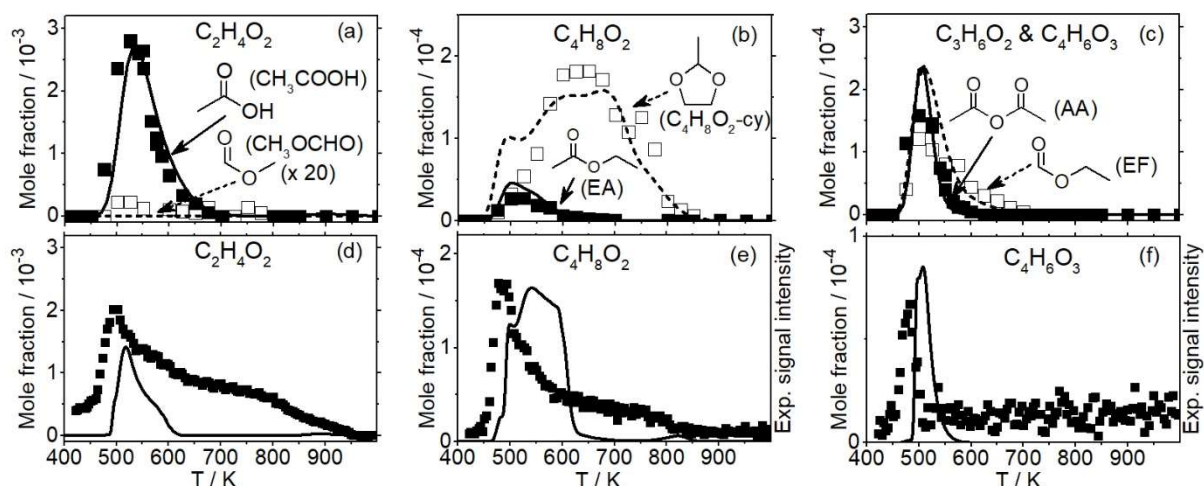


Figure 4: Profiles of intermediates containing 2-3 O-atoms. Symbols: experiment; lines: present model. Top: JSR-GC experiment (a-c); bottom: PFR-EI-MBMS experiment (d-f). In (e) and (f), left axis: simulated mole fraction; right axis: signal intensities (quantification of $C_4H_8O_2$ and $C_4H_6O_3$ was not possible because of lacking EI cross sections).

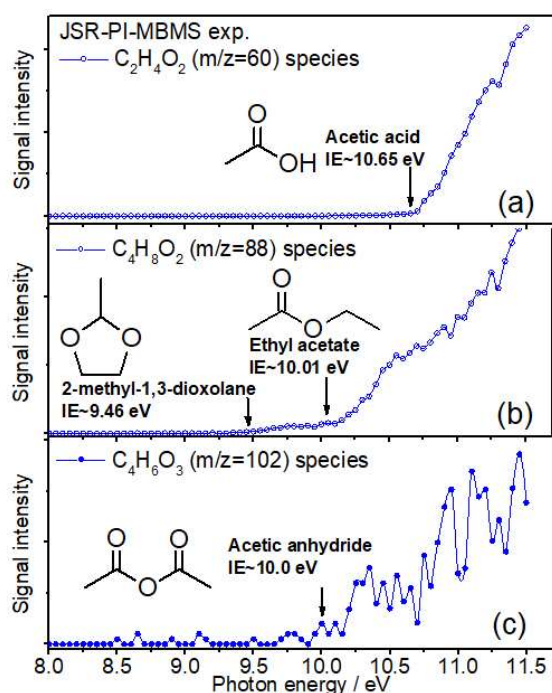


Figure 5: PIE curves of $m/z = 60$ (a), 88 (b), and 102 (c) from the JSR-PI-MBMS experiment at 500 K.

Simulations with the present model included in Figure 4 indicate satisfactory prediction of the formation of intermediates containing 2-3 O-atoms, especially for the most abundant species CH_3COOH . However, our model under-predicts the formation of CH_3OCHO (a low mole fraction species, Figure 4a), indicating that possible unknown additional pathways leading to CH_3OCHO might be missing in the mechanism.

For better understanding the LT chemistry of DEE and the formation of experimentally-observed species, rate of production analyses using the present model at different temperatures (500, 560,

and 700 K) for the studied JSR conditions are presented in Figure 6. Here, H-abstraction reactions by radicals R' (OH , CH_3O , H , etc.) are responsible for DEE consumption. These reactions mainly (~ 92 – 94%) occur at C_α of DEE because of its lowest C–H bond energy ($95.7 \text{ kcal mol}^{-1}$ [5]), yielding the R1 radical (see Figure 6). H-abstractions from C_β (C–H bond energy of $103.2 \text{ kcal mol}^{-1}$) producing the R2 radical account for only 6–8%. The branching ratio of consumption paths of species from R1 and R2 significantly depends on temperature. At HT (700 K), a large fraction of fuel radicals (R1 and R2) is consumed by C–O β -scission forming $\text{CH}_3\text{CHO} + \text{C}_2\text{H}_5$ and $\text{C}_2\text{H}_4 + \text{C}_2\text{H}_5\text{O}$, respectively. At lower temperatures both fuel radicals react largely by O_2 addition leading to the formation of 1-ethoxyethylperoxy (R1OO) and 2-ethoxyethylperoxy (R2OO) radicals, respectively. Under LT conditions, the main consumption path of R1OO leads to the formation of acetic acid (CH_3COOH) through some intermediate steps, explaining why we detected this species with very high amounts. Furthermore, along this consumption path of R1OO, acetic anhydride (AA) is produced via H-abstraction/O–O β -scission from ketohydroperoxide HOOQ1=O (Figure 6). Ethyl formate (EF) and ethyl acetate (EA) are formed via reactions of two R1OO radicals or R1OO with $\text{C}_x\text{H}_y\text{O}_2$ radicals. Several paths following H-abstractions from the C_α positions of DEE lead to the formation of CH_3CHO that was measured with high mole fraction (Table S2, Figure 3). While most detected species are found to be products of H-abstractions at C_α , 2-methyl-1,3-dioxolane ($\text{C}_4\text{H}_8\text{O}_2\text{-cy}$) is mainly formed through H-abstractions at C_β , by the cyclic ether formation process from the Q2OOH radical.

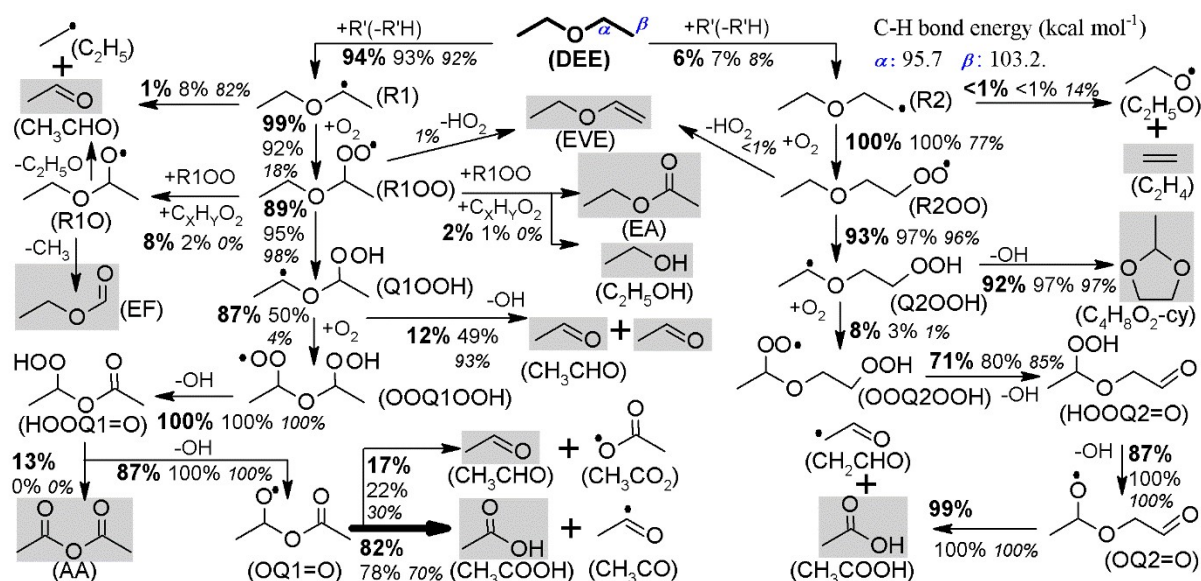


Figure 6: Reaction pathway analysis for the consumption of DEE under the studied JSR conditions using the present model. The experimentally-quantified species are highlighted by shadowed squares. The numbers are percent contribution to the consumption of the species on the source side at different temperatures, coded with different fonts: bold: 500 K, normal: 560 K, italic: 700 K. The thick arrow highlights the main route of acetic acid formation.

5. Conclusions

The present paper reports new experimental data for species profiles measured in the oxidation of DEE at $\phi = 1$ in two nearly-atmospheric reactor types (JSR and PFR) using GC and MBMS techniques. Two NTC zones have been observed. The first NTC zone is an unusual one and mainly results from a competition of the second O_2 addition and the succession of C–O/O–O β -scissions

of the hydroperoxyl-fuel radical (Q10OH). Several intermediates containing 2-3 O-atoms were quantified in the present work and identified as important primary intermediates of the LT oxidation of DEE. A new kinetic model for DEE LT oxidation was established including new reaction classes. Results indicate that the main consumption path of DEE at LT leads mostly to acetic acid and CH_3CO via one of the newly-added reaction classes, contributing to a new picture regarding the LT oxidation of DEE compared to available studies in the literature.

Acknowledgments

The authors wish to thank J.C. Lizardo Huerta for helpful discussions regarding the kinetic model. LST thanks the COST Action CM1404 and the Alexander von Humboldt-Foundation for financial support. Partial support from the Deutsche Forschungsgemeinschaft under project KO1363/31-1 is gratefully acknowledged. The research at SJTU was supported by the National Natural Science Foundation of China (51622605, 91541201) and the Shanghai Science and Technology Committee (No. 17XD1402000).

References

- [1] D.C. Rakopoulos, C.D. Rakopoulos, E.G. Giakoumis, A.M. Dimaratos, *Energy* 43 (1) (2012) 214-224.
- [2] K. Sudheesh, J.M. Mallikarjuna, *Energy* 35 (9) (2010) 3614-3622.
- [3] K. Yasunaga, F. Gillespie, J.M. Simmie, H.J. Curran, Y. Kuraguchi, H. Hoshikawa, M. Yamane, Y. Hidaka, *J. Phys. Chem. A* 114 (34) (2010) 9098-9109.
- [4] M. Werler, L.R. Cancino, R. Schiessl, U. Maas, C. Schulz, M. Fikri, *Proc. Combust. Inst.* 35 (2015) 259-266.
- [5] L.-S. Tran, J. Pieper, H.-H. Carstensen, H. Zhao, I. Graf, Y. Ju, F. Qi, K. Kohse-Höinghaus, *Proc. Combust. Inst.* 36 (2017) 1165-1173.
- [6] F. Gillespie, W.K. Metcalfe, P. Dirrenberger, O. Herbinet, P.-A. Glaude, F. Battin-Leclerc, H.J. Curran, *Energy* 43 (1) (2012) 140-145.
- [7] N. Vin, O. Herbinet, F. Battin-Leclerc, *J. Anal. Appl. Pyrolysis* 121 (2016) 173-176.
- [8] J. Hashimoto, K. Tanoue, N. Taide, Y. Nouno, *Proc. Combust. Inst.* 35 (2015) 973-980.
- [9] K. C. Salooja, *Combust. Flame* 9 (1) (1995) 33-41.
- [10] J. F. Griffiths, T. Inomata, *J. Chem. Soc. Faraday Trans.* 88 (21) (1992) 3153-3158.
- [11] M. Naito, C. Radcliffe, Y. Wada, T. Hoshino, X. Liu, M. Arai, M. Tamura, *J. Loss Prev. Process Ind.* 18 (4) (2005) 469-473.
- [12] D. J. Waddington, *Proc. R. Soc. Lond. A*, 252 (1269) (1959) 260-272.
- [13] S. Di Tommaso, P. Rotureau, O. Crescenzi, C. Adamo, *Phys. Chem. Chem. Phys.* 13 (32) (2011) 14636-14645.
- [14] Y. Sakai, J. Herzler, M. Werler, C. Schulz, M. Fikri, *Proc. Combust. Inst.* 36 (2017) 195-202.
- [15] E. Hu, Y. Chen, Z. Zhang, J.-Y. Chen, Z. Huang, *Fuel* 209 (2017) 509-520.
- [16] Z. Tang, L. Zhang, X. Chen, and G. Tang, *Energy Fuels* 31 (3) (2017) 2803-2813.
- [17] J. Eble, J. Kiecherer, M. Olzmann, *Z. Phys. Chem.* 231 (10) (2017) 1603-1623.
- [18] Y. Sakai, H. Ando, H. K. Chakravarty, H. Pitsch, R. X. Fernandes, *Proc. Combust. Inst.* 35 (2015) 161-169.
- [19] J. Bugler, A. Rodriguez, O. Herbinet, F. Battin-Leclerc, C. Togbé, G. Dayma, P. Dagaut, H. J. Curran, *Proc. Combust. Inst.* 36 (2017) 441-448.

- [20] Z. Zhou, X. Du, J. Yang, Y. Wang, C. Li, S. Wei, L. Du, Y. Li, F. Qi, Q. Wang, J. Synchrotron Rad. 23 (4) (2016) 1035-1045.
- [21] C. Hemken, U. Burke, K.-Y. Lam, D.F. Davidson, R.K. Hanson, K.A. Heufer, K. Kohse-Höinghaus. Combust. Flame 184 (2017) 195-207.
- [22] S. Thion, C. Togbé, Z. Serinyel, G. Dayma, P. Dagaut, Combust. Flame 185 (2017) 4-15.
- [23] A. Jalan, I.M. Alecu, R. Meana-Pañeda, J. Aguilera-Iparraguirre, K.R. Yang, S.S. Merchant, D.G. Truhlar, W.H. Green, J. Am. Chem. Soc. 135 (30) (2013) 11100-11114.
- [24] Z. Wang, X. Zhang, L. Xing, L. Zhang, F. Herrmann, K. Moshhammer, F. Qi, K. Kohse-Höinghaus, Combust. Flame 162 (4) (2015) 1113-1125.
- [25] C.W. Gao, J.W. Allen, W.H. Green, R.H. West, Comput. Phys. Commun. 203 (2016) 212-225.
- [26] A. Cuoci, A. Frassoldati, T. Faravelli, E. Ranzi, Comput. Phys. Commun. 192 (2015) 237-264.
- [27] NIST Chemistry WebBook, available at < <http://webbook.nist.gov/chemistry/>>.
- [28] A. Rodriguez, O. Herbinet, Z. Wang, F. Qi, C. Fittschen, P.R. Westmoreland, F. Battin-Leclerc. Proc. Combust. Inst. 36 (2017) 333-342.